

Consequences of Lattice Mismatch for Phase Equilibrium in Heterostructured Solids

Layne B. Frechette 

*Department of Chemistry, University of California, Berkeley, California 94720, USA
and Erwin Schrödinger Institute for Mathematics and Physics,
University of Vienna, Boltzmannngasse 9, Wien 1090, Austria*

Christoph Dellago

*Faculty of Physics, University of Vienna, Boltzmannngasse 5, Wien 1090, Austria
and Erwin Schrödinger Institute for Mathematics and Physics,
University of Vienna, Boltzmannngasse 9, Wien 1090, Austria*

Phillip L. Geissler*

*Department of Chemistry, University of California, Berkeley, California 94720, USA
and Erwin Schrödinger Institute for Mathematics and Physics,
University of Vienna, Boltzmannngasse 9, Wien 1090, Austria*



(Received 21 June 2019; published 24 September 2019)

Lattice mismatch can substantially impact the spatial organization of heterogeneous materials. We examine a simple model for lattice-mismatched solids over a broad range of temperature and composition, revealing both uniform and spatially modulated phases. Scenarios for coexistence among them are unconventional due to the extensive mechanical cost of segregation. Together with an adapted Maxwell construction for elastic phase separation, mean field theory predicts a phase diagram that captures key low-temperature features of Monte Carlo simulations.

DOI: [10.1103/PhysRevLett.123.135701](https://doi.org/10.1103/PhysRevLett.123.135701)

Lattice mismatch—the difference in preferred bond length between adjoining regions of a heterogeneous solid—is a natural consequence of mixing diverse components to build complex materials. It is well recognized that juxtaposing domains with different lattice spacings introduces local strain, significantly impacting material properties such as electronic structure [1–3] and the propensity to form dislocations [4,5]. The resulting elastic energy can also significantly bias the spatial arrangement of compositional defects and interfaces. How these biases influence the thermodynamic stability of mixed phases, however, has not been thoroughly characterized. Here, we examine the phase behavior of a microscopic model for such systems, motivated by intriguing heterostructures adopted by CdS/Ag₂S nanocrystals [6] in the course of cation exchange reactions [7–10]. Their alternating stripes of Cd-rich and Ag-rich domains have been attributed to a lattice mismatch between the CdS and Ag₂S domains [11], but an understanding of how they form, and whether they are thermodynamically stable, has been lacking.

Our model and analysis draw from those introduced by Fratzl and Penrose [12,13], who represented a two-component solid by atoms on a flexible square lattice with bond length preferences that depend on local composition. By integrating out mechanical fluctuations, they obtained an approximate effective Hamiltonian for the composition field, whose atomic identities interact in a pairwise and anisotropic

fashion. For the special case of a 1:1 mixture of the two species, they used mean field theory (MFT) to predict a second-order phase transition between a high-temperature disordered phase and a low-temperature ordered phase characterized by stripes of alternating composition.

This Letter surveys the composition-temperature phase diagram of a similar model much more broadly, revealing an unanticipated richness with interesting implications for nanoscale transformations. Monte Carlo (MC) simulations confirm the predicted appearance of modulated-order phases with spontaneously broken symmetry. They further point to unusual scenarios of phase separation, with well-defined interfaces but a nonconvex free energy. This behavior can be understood as a consequence of elastic energies for phase separation that scale extensively with system size. For this situation we devise a procedure, akin to the conventional Maxwell construction, to determine the boundaries of coexistence regions given equations of state for the corresponding bulk phases. Although the high temperature phase behavior is dominated by fluctuations on the triangular lattice, a straightforward mean field theory describes the required bulk properties quite faithfully at low temperature. We combine these approaches to predict a phase diagram that accounts for the full set of structures observed in our MC simulations, including those with system-spanning interfaces.

We consider a model in which N atoms are situated near the sites of a completely occupied two-dimensional

triangular lattice, with periodic boundary conditions in both Cartesian directions. The atom at site \mathbf{R} has two possible types, indicated as $\sigma_{\mathbf{R}} = +1$ (type A) and $\sigma_{\mathbf{R}} = -1$ (type B). These atom types are distinguished by their size, so that nearest neighbor atoms at sites \mathbf{R} and $\mathbf{R} + a\hat{\alpha}$ prefer a bond distance l dictated by their identities,

$$l(\sigma_{\mathbf{R}}, \sigma_{\mathbf{R}+a\hat{\alpha}}) = \begin{cases} l_{AA}, & \text{for } \sigma_{\mathbf{R}} = \sigma_{\mathbf{R}+a\hat{\alpha}} = 1, \\ l_{AB}, & \text{for } \sigma_{\mathbf{R}} \neq \sigma_{\mathbf{R}+a\hat{\alpha}}, \\ l_{BB}, & \text{for } \sigma_{\mathbf{R}} = \sigma_{\mathbf{R}+a\hat{\alpha}} = -1, \end{cases} \quad (1)$$

where a is the lattice constant and $\hat{\alpha}$ is a unit bond vector. We take $l_{BB} < l_{AA}$ and adopt the simple mixing rule $l_{AB} = (l_{AA} + l_{BB})/2$. The lattice mismatch $\Delta = (l_{AA} - l_{BB})/2$ will serve as our basic unit of length.

Both the atoms' identities and their displacements ($\mathbf{u}_{\mathbf{R}}$) away from ideal lattice positions fluctuate according to a Boltzmann distribution $P(\{\mathbf{u}_{\mathbf{R}}\}, \{\sigma_{\mathbf{R}}\}) \propto e^{-\beta\mathcal{H}}$, where $T = (k_B\beta)^{-1}$ is temperature and $\mathcal{H}(\{\mathbf{u}_{\mathbf{R}}\}, \{\sigma_{\mathbf{R}}\})$ is the energy of a given configuration. The net displacement $\sum_{\mathbf{R}} \mathbf{u}_{\mathbf{R}} = 0$ and the net fraction of A atoms $c = (2N)^{-1} \sum_{\mathbf{R}} (\sigma_{\mathbf{R}} + 1)$ are both implicitly held fixed. Fluctuations in the lattice constant a (at zero external pressure), however, are included in the ensemble we consider; for large systems and small lattice mismatch, this freedom primarily allows the macroscopic geometry to adapt to the imposed composition, $a \approx l_{AB} + \Delta(2c - 1) + O(N^{-1/2})$. The free energy $F(c)$ for this ensemble encodes the model's response to changing proportions of atom types, and in particular its phase transitions.

Deviations of bond distances away from their locally preferred lengths incur energy that grows quadratically,

$$\mathcal{H} = \frac{K}{4} \sum_{\mathbf{R}, \hat{\alpha}} [|a\hat{\alpha} + \mathbf{u}_{\mathbf{R}} - \mathbf{u}_{\mathbf{R}+a\hat{\alpha}}| - l(\sigma_{\mathbf{R}}, \sigma_{\mathbf{R}+a\hat{\alpha}})]^2, \quad (2)$$

where K is a positive constant that sets the natural energy scale $\epsilon = K\Delta^2/8$. All energies and lengths will henceforth be expressed in units of ϵ and Δ , respectively. The ground states of Eq. (2) clearly occur in the absence of heterogeneity, i.e., $c = 0$ or $c = 1$. At intermediate composition, fixed connectivity prevents the collection of bonds from simultaneously attaining their preferred lengths. We have explored the resulting compositional correlations analytically using small-mismatch and mean-field approximations, and also numerically using MC simulations.

At a high temperature, equilibrium states of this model are macroscopically uniform but exhibit suggestive microscopic correlations. A few such disordered configurations, selected randomly from MC simulations, are shown in the top row of Fig. 1(a). For nearly pure mixtures at modest T (≈ 1.4) defects cluster in space, but not compactly. Motifs of microscopically alternating composition are even more evident at intermediate net composition, where typical equilibrium states resemble interpenetrating networks

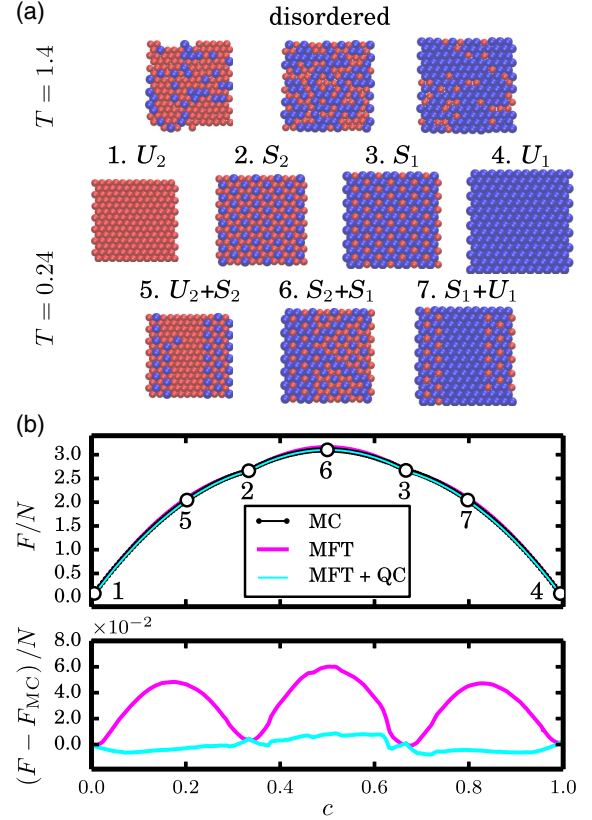


FIG. 1. Monte Carlo (MC) simulation results for the elastic model in Eq. (2). (a) Survey of configurations exemplifying the disordered, unstructured (U_1 and U_2), and superlattice (S_1 and S_2) phases. Blue and red spheres represent A and B atoms, respectively. (b) Free energy per particle $F(c)/N$ as a function of composition c at $T = 0.24$. Circles numbered 1 to 7 refer to the corresponding configurations in (a). Results are shown in black for MC sampling, in pink for the mean field theory (MFT) of Eq. (5), and in blue for the application of the quadratic construction [QC, Eq. (7)] to mean-field thermodynamics. Lower panel shows the difference between MFT and MC results (pink), and the difference between MFT + QC and MC (blue).

of A and B atoms. At low temperatures these structural tendencies produce four phases. The “superlattice” phases S_1 and S_2 feature periodic modulation of atom types with wavelengths on the order of a single lattice spacing. In the vein of previous studies of modulated order [14,15] we characterize these phases by their average composition on three distinct sublattices. In S_1 two sublattices are enriched in atom type A, while the third is enriched in type B. The roles of A and B are reversed in S_2 . The ideal forms of these phases, where the net composition per site $2c_\gamma - 1 = (3/N) \sum_{\mathbf{R}}^{(\gamma)} \sigma_{\mathbf{R}}$ is ± 1 on each sublattice γ , occur at $c = 1/3$ and $c = 2/3$. In the “unstructured” phases U_1 and U_2 , whose zero-temperature forms are compositionally pure, the average composition is independent of the sublattice. Previous work anticipated the appearance of modulated order phases like S_1 and S_2 [12,13], but not their competition with unstructured phases.

The emergence of superlattice phases as temperature decreases at intermediate composition involves a breaking of symmetry between A - and B -rich states. This symmetry is suggested by the form of Eq. (2), but not precisely implied. Despite its Hookean form, \mathcal{H} is an anharmonic function of atomic displacements, with nonlinearities of order Δ/a that favor one atom type (B) for all $c \neq 0, 1$. Symmetry with respect to a global transformation of the composition $\{\sigma_{\mathbf{R}}\} \rightarrow \{-\sigma_{\mathbf{R}}\}$ is thus not guaranteed. Nevertheless, MC simulations suggest a symmetry of thermodynamic quantities about c very near $1/2$ even for the substantial lattice mismatch $\Delta/a = 0.15$, indicating that nonlinearities in \mathcal{H} are intrinsically weak in effect [16].

MC sampling further reveals states of coexistence among these four phases, as depicted in the bottom row of Fig. 1(a). Specifically, S_1 and S_2 coexist at low temperatures over a range of compositions centered near $c = 1/2$. Coexistence between S_1 and U_1 , and between S_2 and U_2 , are also observed. But under no conditions do simulations exhibit coexistence between U_1 and U_2 .

The usual quantitative signature of phase separation in d spatial dimensions is a subextensive nonconvexity in the corresponding free energy, i.e., a barrier of $O(N^{-(d-1)/d})$ in $F(c)/N$ as a function of c that approaches the convex envelope in the thermodynamic limit. The free energies $F_{\text{MC}}(c)$ we have determined from simulation (using methods of umbrella sampling and histogram reweighting [17–19]) do not follow this expectation. Specifically, plots of $F_{\text{MC}}(c)/N$ in Fig. 1(b) show nonconvex regions that persist as N becomes large [20]. We will argue that this behavior is generic to the coexistence of geometrically mismatched solids with a fixed macroscopic shape, and that the resulting negative curvature of $F(c)$ is simply related to their elastic properties.

For atom types that differ only slightly in size, $\Delta/a \ll 1$, the energy \mathcal{H} is approximately quadratic in the displacement field $\mathbf{u}_{\mathbf{R}}$. Mechanical fluctuations in this Gaussian limit can be integrated out exactly [12,20], yielding marginal statistics of the composition field that corresponds to a Boltzmann distribution with effective energy

$$\mathcal{H}_{\text{eff}}(\{\sigma_{\mathbf{R}}\}) = \frac{1}{2N} \sum_{\mathbf{q}} \tilde{V}_{\mathbf{q}} |\tilde{\sigma}_{\mathbf{q}}|^2 = \frac{1}{2} \sum_{\mathbf{R}, \mathbf{R}' \neq \mathbf{R}} \sigma_{\mathbf{R}} V_{\mathbf{R}-\mathbf{R}'} \sigma_{\mathbf{R}'}, \quad (3)$$

where $\tilde{f}_{\mathbf{q}} = \sum_{\mathbf{R}} f_{\mathbf{R}} e^{-i\mathbf{q}\cdot\mathbf{R}}$ denotes the Fourier transform of a generic function $f_{\mathbf{R}}$. The effective interaction potential $V_{\mathbf{R}}$ for compositional fluctuations has Fourier components that depend smoothly on the wave vector \mathbf{q} at all finite wavelengths:

$$\tilde{V}_{\mathbf{q}} = \frac{4(2 \cos \frac{q_x a}{2} \cos \frac{\sqrt{3} q_y a}{2} + \cos q_x a - 3)^2}{(\cos q_x a - 2)(4 \cos \frac{q_x a}{2} \cos \frac{\sqrt{3} q_y a}{2} - 3) + \cos \sqrt{3} q_y a}, \quad (4)$$

where x and y indicate Cartesian components. $\tilde{V}_{\mathbf{q}}$ vanishes abruptly at $\mathbf{q} = 0$, with important implications for open ensembles in which c can vary; here, at fixed net composition, the value of \tilde{V}_0 is irrelevant.

Figure 2 shows the effective compositional potential in both real- and reciprocal-space representations. Like the result of Ref. [12] for more complicated mechanical coupling on a square lattice, $\tilde{V}_{\mathbf{q}}$ has local minima near the boundary of the first Brillouin zone. Periodic variations in composition are thus the least costly at microscopic wavelengths and along particular lattice directions, echoing the stability of superlattice phases observed in simulations. The modulated microstructure of these phases is suggested even more strongly by the dependence of $V_{\mathbf{R}}$ on atom separation, which we obtain by numerical inversion of the Fourier transform. Elastic interactions clearly disfavor the placement of defects on neighboring lattice sites [20].

The effective Hamiltonian $\mathcal{H}_{\text{eff}}(\{\sigma_{\mathbf{R}}\})$ for compositional fluctuations can serve as the basis for a simple MFT. Following standard treatments [15,33], we consider a reference system of noninteracting spins in an external field that may differ among the three sublattices. Variational optimization of this reference system yields a set of

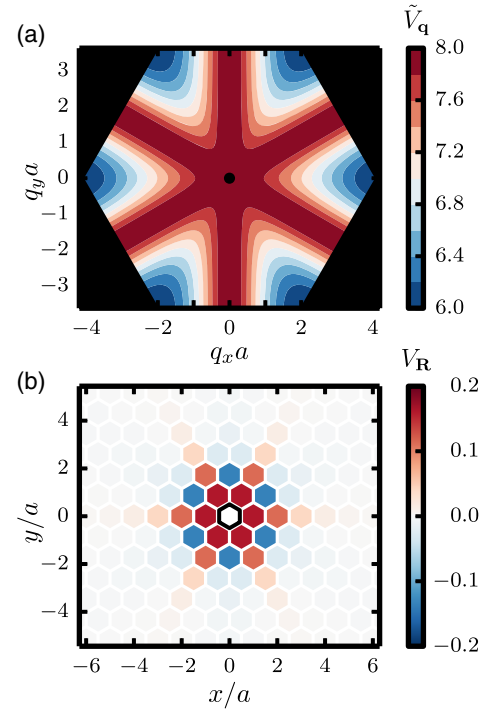


FIG. 2. Effective pair potential V for the composition field in the small-mismatch approximation of Eq. (3). (a) Reciprocal space representation $\tilde{V}_{\mathbf{q}}$, plotted in the first Brillouin zone. The black dot in the center indicates the discontinuity at $\mathbf{q} = \mathbf{0}$, where $\tilde{V}_0 = 0$. (b): Effective interaction between an A (or B) atom at the origin (marked by the outlined hexagon) and another A (or B) atom at \mathbf{R} . Mixed interactions between A and B have opposite signs.

self-consistent equations for the average compositions c_γ on sublattices $\gamma = 1, 2, 3$,

$$2c_\gamma - 1 = \tanh\beta \left(\mu - 2 \sum_{\delta=1}^3 (2c_\delta - 1) J_{\gamma\delta} \right), \quad (5)$$

where μ is a Lagrange multiplier enforcing the constraint $c = \sum_\gamma c_\gamma / 3$, and

$$J_{\gamma\delta} = \frac{3}{N} \sum_{\mathbf{R}}^{(\gamma)} \sum_{\mathbf{R}' \neq \mathbf{R}}^{(\delta)} V_{\mathbf{R}, \mathbf{R}'} \quad (6)$$

describes the net coupling between sublattices γ and δ .

We solve Eq. (5) numerically to determine an estimate $F_{\text{MFT}}(c)$ for the free energy. This mean-field approximation successfully captures some of the general features of our simulation results, particularly at low temperature. For the example plotted in Fig. 1(b), discrepancies are small over the entire range of c , and significant only where simulations show two phases coexisting in similar proportions. Since the states considered in MFT are macroscopically uniform by construction, a failure to describe phase equilibrium is expected. From such a theory of uniform states, assessing the thermodynamics of coexistence would typically proceed by Maxwell construction, removing nonconvex regions of $F_{\text{MFT}}(c)$ that usually signal instability to the formation of interfaces. For a case in which the true free energy is nonconvex, a different procedure is clearly needed. As has been noted previously in the context of capillary wave suppression in elastic solids [34], here we must specifically acknowledge an extensive thermodynamic penalty to accommodate domains with differing lattice constants in a rectangular macroscopic geometry.

Linear elasticity theory associates an energy $E = Y(L - L_0)^2$ with deforming a solid from its natural length L_0 to a length L , where Y is Young's modulus [35,36]. From this rule we can estimate the cost of phase coexistence in a lattice-mismatched solid. Consider two phases with compositions c_1 and c_2 , whose macroscopically uniform realizations have free energies per particle $f(c_1)$ and $f(c_2)$. In the Supplemental Material [20] we estimate the free energy of a solid in which domains of these phases coexist at a net composition c :

$$\frac{F_{\text{coex}}(c_1, c_2; c)}{N} = f(c_1) - \frac{\Delta c_1}{\Delta c_2 - \Delta c_1} \Delta f - Y \Delta l^2 \Delta c_1 \Delta c_2. \quad (7)$$

Here, $\Delta c_j = c_j - c$, $\Delta f = f(c_2) - f(c_1)$, $\Delta l = l(c_1) - l(c_2)$, and $l(c_j)$ is the energy-minimizing unit cell length for composition c_j .

Absent lattice mismatch ($\Delta l = 0$), minimizing Eq. (7) with respect to c_1 and c_2 (at fixed c) corresponds to the conventional double-tangent construction. For $\Delta l \neq 0$,

coexistence instead entails a free energy that connects points $[c_1^*, f(c_1^*)]$ and $[c_2^*, f(c_2^*)]$ in the $c - f$ plane with a parabola of curvature $\kappa_{\text{coex}} = -Y \Delta l^2$. We term this procedure the ‘‘quadratic construction’’ (QC) [20].

Applying the QC to our MFT estimate $F_{\text{MFT}}(c)$, correspondence with MC results can be greatly improved. In the case of Fig. 1(b), mean-field predictions for $F(c)$ deviate from simulations by less than 1%, comparable to random sampling error. This excellent agreement emphasizes a predominance of macroscopically heterogeneous states in the temperature range $T \lesssim 0.4$, despite the nonconvexity of $F(c)$. We attribute this agreement to the appreciable spatial range of $V_{\mathbf{R}}$, which includes substantial coupling between sites separated by several lattice spacings. The low- \mathbf{q} form of $\tilde{V}_{\mathbf{q}}$, which varies quadratically with q to lowest order, suggests an eventual failure of MFT near criticality [20,37]. Quantitative agreement indeed deteriorates with increasing temperature, and above $T \approx 0.46$ the fluctuations neglected by MFT influence phase behavior even qualitatively. The phase diagram for our elastic model, as determined from MC simulations [20] and plotted in Fig. 3(b), is equivalent in form to a spin model on the same lattice with couplings that resemble $V_{\mathbf{R}}$ at short range [14]. In contrast to predictions of MFT [see Fig. 3(a)] (i) the loss of superlattice

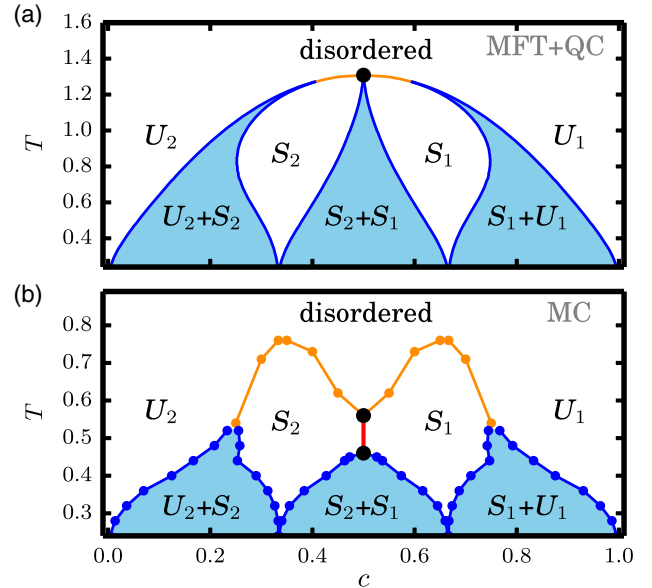


FIG. 3. Phase diagram for our elastic model in the plane of temperature and composition. (a) Mean-field prediction resulting from the quadratic construction of Eq. (7). Black circle indicates a critical point at $T \approx 1.3$; elsewhere, lines indicate first-order transitions. Orange lines separate the disordered phase from superlattice phases S_1 or S_2 . Blue lines bound coexistence regions, which are shaded in light blue. (b) Numerically exact results from Monte Carlo sampling. In this case, the disordered-to-superlattice transitions (orange lines) are continuous. A line of Kosterlitz-Thouless critical points between $T_c^{\text{lower}} \approx 0.46$ and $T_c^{\text{upper}} \approx 0.56$ is shown in red.

order upon heating is continuous, with critical properties belonging to the three-state Potts model universality class, and (ii) in the temperature range $T \approx 0.46$ to $T \approx 0.56$, phases S_1 and S_2 are separated by a line of Kosterlitz-Thouless critical points. Away from these exotic features, first-order transitions are well described by Eqs. (5) and (7). The absence of a first-order transition between unstructured phases U_1 and U_2 is also captured by MFT and the QC, which manifests an energetic instability for this scenario [20].

Our results demonstrate that lattice mismatch can generate more nuanced thermodynamic behaviors than was previously appreciated. They also indicate a central importance of lattice geometry and boundary conditions. The modulated order of phases S_1 and S_2 owes its stability to the fixed macroscopic shape implied by periodic boundary conditions. Such a constraint on boundary shape could arise in real systems from strong interactions that bind a nanocrystal to a substrate, a notion consistent with the observation of stable Cu superlattices within two-dimensional Bi_2Se_3 nanocrystals [38]. It could also be imposed by core-shell interactions in hetero-nanostructures, a possibility which we have explored with MC simulations [20]. Core-shell arrangements, moreover, are natural intermediates in the course of exchange reactions that proceed most rapidly at surface sites [39].

The precise form of the phase diagram in Fig. 3(b) is likely specific to the dimensionality and lattice symmetry of the elastic model we have studied. Several of its interesting features, however, we expect to be general for heterostructured solids under appropriate boundary conditions. A tendency for modulated order, for example, is evident in three-dimensional systems explored previously [40] and in exploratory simulations described in the Supplemental Material [20]. Thermodynamic potentials with indefinite convexity, and their implications for phase coexistence, are similarly anticipated as generic consequences of the elastic forces attending lattice mismatch. Testing these predictions in the laboratory may be the most straightforward for materials that can be manipulated more readily than the internal structure of nanocrystals, for instance assemblies of DNA-coated nanoparticles [41] or spin-crossover compounds [42–47], where elasticity is known to play a significant role.

We thank Jaffar Hasnain for stimulating conversations. This work was supported by National Science Foundation (NSF) Grant No. CHE-1416161. This research also used resources of the National Energy Research Scientific Computing Center (NERSC), a U.S. Department of Energy Office of Science User Facility operated under Contract No. DE-AC02-05CH11231. P.L.G. and L.B.F. acknowledge stays at the Erwin Schrödinger Institute for Mathematics and Physics at the University of Vienna.

*geissler@berkeley.edu

- [1] A. M. Smith, A. M. Mohs, and S. Nie, *Nat. Nanotechnol.* **4**, 56 (2009).
- [2] S.-M. Choi, S.-H. Jhi, and Y.-W. Son, *Phys. Rev. B* **81**, 081407(R) (2010).
- [3] V. M. Pereira and A. H. Castro Neto, *Phys. Rev. Lett.* **103**, 046801 (2009).
- [4] J. Matthews and A. Blakeslee, *J. Cryst. Growth* **27**, 118 (1974).
- [5] R. People and J. C. Bean, *Appl. Phys. Lett.* **47**, 322 (1985).
- [6] R. D. Robinson, B. Sadler, D. O. Demchenko, C. K. Erdonmez, L.-W. Wang, and A. P. Alivisatos, *Science* **317**, 355 (2007).
- [7] D. H. Son, S. Hughes, Y. Yin, and A. Alivisatos, *Science* **306**, 1009 (2004).
- [8] H. Li, M. Zanella, A. Genovese, M. Povia, A. Falqui, C. Giannini, and L. Manna, *Nano Lett.* **11**, 4964 (2011).
- [9] J. B. Rivest and P. K. Jain, *Chem. Soc. Rev.* **42**, 89 (2013).
- [10] L. De Trizio and L. Manna, *Chem. Rev.* **116**, 10852 (2016).
- [11] D. O. Demchenko, R. D. Robinson, B. Sadler, C. K. Erdonmez, A. P. Alivisatos, and L.-W. Wang, *ACS Nano* **2**, 627 (2008).
- [12] P. Fratzl and O. Penrose, *Acta Metall. Mater.* **43**, 2921 (1995).
- [13] P. Fratzl and O. Penrose, *Acta Mater.* **44**, 3227 (1996).
- [14] D. P. Landau, *Phys. Rev. B* **27**, 5604 (1983).
- [15] T. DeSimone, R. M. Stratt, and J. Tobochnik, *Phys. Rev. B* **32**, 1549 (1985).
- [16] As one factor limiting the effects of nonlinearity, the displacement field \mathbf{u}_R is identically zero for all four phases in their zero-temperature form.
- [17] D. Frenkel and B. Smit, *Understanding Molecular Simulation: From Algorithms to Applications* 2nd ed. (Academic Press, San Diego, 2001), Chap. 7.
- [18] G. Torrie and J. Valleau, *J. Comput. Phys.* **23**, 187 (1977).
- [19] S. Kumar, J. M. Rosenberg, D. Bouzida, R. H. Swendsen, and P. A. Kollman, *J. Comput. Chem.* **13**, 1011 (1992).
- [20] See Supplemental Material at <http://link.aps.org/supplemental/10.1103/PhysRevLett.123.135701>, which includes Refs. [21–32], for derivations of results in the text, simulation protocols, and supporting calculations.
- [21] N. Mermin and N. Ashcroft, *Solid State Physics* (Saunders College, Philadelphia, 1976), Chap. 5.
- [22] M. Matsumoto and T. Nishimura, *ACM Trans. Model. Comput. Simul.* **8**, 3 (1998).
- [23] F. R. M. Galassi, J. Davies, J. Theiler, B. Gough, G. Jungman, P. Alken, and M. Booth, *GNU Scientific Library Reference Manual* 3rd ed (Network Theory Ltd., Bristol, 2009).
- [24] K. Kawasaki, *Phys. Rev.* **145**, 224 (1966).
- [25] E. Jones, E. Oliphant, P. Peterson *et al.*, *SciPy: Open source scientific tools for Python*, 2001.
- [26] R. Brent, *Algorithms for Minimization Without Derivatives* (Prentice-Hall, Englewood Cliffs, 1973), Chaps. 3–4.
- [27] M. F. Thorpe and E. J. Garboczi, *Phys. Rev. B* **42**, 8405 (1990).
- [28] G. A. Baker and J. W. Essam, *J. Chem. Phys.* **55**, 861 (1971).
- [29] S. Alexander, *Phys. Lett. A* **54**, 353 (1975).
- [30] J. D. Noh and D. Kim, *Int. J. Mod. Phys. B* **06**, 2913 (1992).
- [31] K. Binder, *Phys. Rev. Lett.* **47**, 693 (1981).

- [32] J. Cardy, *Scaling and Renormalization in Statistical Physics* (Cambridge University Press, Cambridge, England, 1996), Chap. 1.
- [33] D. Chandler, *Introduction to Modern Statistical Mechanics* (Oxford University Press, New York, 1987), Chap. 5.
- [34] B. J. Schulz, B. Dünweg, K. Binder, and M. Müller, *Phys. Rev. Lett.* **95**, 096101 (2005).
- [35] L. Landau and E. Lifshitz, *Theory of Elasticity* 3rd ed. (Butterworth-Heinemann, Oxford, 1986), Chap. 1.
- [36] R. Phillips, J. Kondev, and J. Theriot, *Physical Biology of the Cell* 1st ed. (Garland Science, New York and Oxford, 2009), Chap. 10.
- [37] M. E. Fisher, S.-k. Ma, and B. G. Nickel, *Phys. Rev. Lett.* **29**, 917 (1972).
- [38] J. Buha and L. Manna, *Chem. Mater.* **29**, 1419 (2017).
- [39] E. Groeneveld, L. Witteman, M. Lefferts, X. Ke, S. Bals, G. Van Tendeloo, and C. de Mello Donega, *ACS Nano* **7**, 7913 (2013).
- [40] H. Gupta, *Acta Mater.* **49**, 53 (2001).
- [41] P. A. Gabrys, S. E. Seo, M. X. Wang, E. Oh, R. J. Macfarlane, and C. A. Mirkin, *Nano Lett.* **18**, 579 (2018).
- [42] C. Enachescu, M. Nishino, S. Miyashita, K. Boukheddaden, F. Varret, and P. A. Rikvold, *Phys. Rev. B* **91**, 104102 (2015).
- [43] T. Nakada, T. Mori, S. Miyashita, M. Nishino, S. Todo, W. Nicolazzi, and P. A. Rikvold, *Phys. Rev. B* **85**, 054408 (2012).
- [44] W. Nicolazzi and S. Pillet, *Phys. Rev. B* **85**, 094101 (2012).
- [45] M. Nishino, K. Boukheddaden, Y. Konishi, and S. Miyashita, *Phys. Rev. Lett.* **98**, 247203 (2007).
- [46] A. Slimani, K. Boukheddaden, F. Varret, H. Oubouchou, M. Nishino, and S. Miyashita, *Phys. Rev. B* **87**, 014111 (2013).
- [47] H. Spiering and N. Willenbacher, *J. Phys. Condens. Matter* **1**, 10089 (1989).